ATMOSPHERIC SCIENCE LETTERS
Atmos. Sci. Let. **6**: 118–122 (2005)
Published online 28 April 2005 in Wiley InterScience (www.interscience.wiley.com). **DOI:** 10.1002/asl.100

On physical realizability and uncertainty of numerical solutions

Andreas Dörnbrack,[1]* James D. Doyle,[2] Todd P. Lane,[3] Robert D. Sharman[3] and Piotr K. Smolarkiewicz[3]
[1] *DLR Oberpfaffenhofen, Institut für Physik der Atmosphäre, Wessling, Germany*
[2] *Marine Meteorological Division, Naval Research Laboratory, Monterey, CA, USA*
[3] *National Center for Atmospheric Research[1], P.O. Box 3000, Boulder, CO, USA*

**Correspondence to:*
Andreas Dörnbrack, DLR Oberpfaffenhofen, Institut für Physik der Atmosphäre, D-82230 Wessling, Germany.
E-mail: andreas.doernbrack@dlr.de

Received: 2 November 2004
Revised: 24 January 2005
Accepted: 24 January 2005

Abstract

Numerical experiments of the stratified flow past a bell-shaped mountain with a shallow shear layer aloft are performed. Two different approximations of the entropy equation (explicit vs implicit numerical treatment of gravity waves) lead to a substantial discrepancy of the numerical results. As the flow is metastable, it turns out that both solutions are physically realizable and the quality of the solution changes in response to small variations in the accuracy of the numerical approximation. Copyright © 2005 Royal Meteorological Society

Keywords: computational fluid dynamics; numerical methods; atmospheric dynamics; orographic flow

1. Motivation

It is widely recognized that truncation errors of under-resolved numerical solutions can appear as physically realizable phenomena; conspicuous examples are numerical diffusion and dispersion of advection schemes. As the systems of addressed PDEs become more complicated, spurious solutions can take a more subtle form. For example, Smolarkiewicz and Clark (1986) reveal spurious lee waves due to unbalanced temporal truncation errors of advective velocities; whereas Héreil and Laprise (1996), and later Grabowski and Smolarkiewicz (2002), show spurious tilt of a hydrostatic vertically propagating mountain wave due to the outsized integration time step. Recently, Klemp *et al*. (2003) discussed the gravity-wave test proposed by Schär *et al*. (2002), and explained the solution bifurcation into a spurious state in terms of the incompatibility of finite-difference approximations of various terms in the equations of motion. Spurious structures with realistic appearance are not only limited to wave dynamics but are also reported for purely vortical flows. One example is a double shear-layer roll-up — a computational benchmark of Bell *et al*. (1989) — where numerical solutions take the form of either two or three eddies, depending on numerical method employed; cf. Drikakis and Smolarkiewicz (2001). Noteworthy, Drikakis *et al*. (2002) argued that both solutions are meaningful: while the two eddies are correct but metastable, the three eddies are physically realizable.

Here, we report a series of experiments for which two different approximations of the entropy equation result in a substantial discrepancy of numerical solutions. The principal setup of the experiment was motivated by a COAMPS simulation of sheared Alpine flow, which produced unexpected coherent 'horizontal rolls'. To investigate the realizability of the solution, an idealized scenario was designed: the nonrotating, stratified 3D flow past a bell-shaped mountain with a shallow layer of 90° directional wind shear aloft — an exaggeration of the problem studied by Shutts and Gadian (1999, SG99). The COAMPS solution to the idealized problem evinces fine-scale horizontally elongated updrafts and downdrafts in the lee of the mountain, with wave fronts almost perpendicular to the hydrostatic response.

Our numerical model — highlighted in the following section — accurately reproduces the results of SG99. However, as the nonlinearity of the problem (viz. the forcing amplitude) increases, the solution becomes sensitive to details of the numerics. For the exaggerated problem, the different numerical approximations diverge. One solution evinces a compact 3D gravity-wave pattern, whereas another shows in addition small-scale horizontally elongated structures like those simulated with COAMPS. Because the analytic solution is unknown, and a conclusive convergence study is unaffordable, it is *a priori* unclear which solution is correct, and which is merely a numerical artifact in disguise of physical effect. On the basis of extensive numerical experimentation, we argue that both are physically realizable. It turns out that the flow studied is metastable, and the quality of the solution changes in response to small variations in the accuracy of numerical representation.

[1] NCAR is sponsored by the National Science Foundation

2. Numerical method

Our numerical experiments are performed with the nonhydrostatic anelastic model EULAG. An up-to-date comprehensive description of the model and its capabilities can be found in Prusa and Smolarkiewicz (2003), and Smolarkiewicz and Prusa (2005). The governing equations are solved by means of finite-difference approximations using a second-order accurate nonoscillatory forward-in-time (NFT) approach (Smolarkiewicz and Margolin, 1997). In the following, we summarize shortly the essential aspects of the scheme while focusing on the differences between the implicit and explicit numerical treatment of gravity waves.

The prognostic equations are written compactly in a conservation-law form

$$\frac{\partial \rho^* \Psi}{\partial t} + \nabla\cdot(\rho^* \mathbf{v} \Psi) = \rho^* R^\Psi, \tag{1}$$

where ρ^* is the reference density multiplied by the Jacobian of coordinate transformation, $\nabla := (\partial/\partial x, \partial/\partial y, \partial/\partial z)$, Ψ symbolizes the velocity components u, v, and w or the potential temperature Θ, and R^Ψ denotes the associated rhs (e.g. a total of the pressure gradient force and buoyancy, for momenta). On a discrete mesh, the NFT approximation of (1) is written as

$$\Psi_{\mathbf{i}}^{n+1} = LE_{\mathbf{i}}(\widetilde{\Psi}) + 0.5\Delta t R^\Psi|_{\mathbf{i}}^{n+1}, \tag{2}$$

where $\Psi_{\mathbf{i}}^{n+1}$ denotes the solution at the grid point $(t^{n+1}, \mathbf{x}_\mathbf{i})$, $\widetilde{\Psi} := \Psi^n + 0.5\Delta t R^\Psi|^n$, and LE denotes the NFT transport operator. In the Eulerian scheme, used exclusively in this paper, LE integrates the homogeneous transport Equation (1) — viz., LE advects $\widetilde{\Psi}$ using a fully second-order-accurate flux-form scheme MPDATA (for a review, see Smolarkiewicz and Margolin, 1998).

For adiabatic motions considered in this note, in the model option explicit with respect to gravity waves, $R^\Theta \equiv 0$ and $\widetilde{\Theta} \equiv \Theta$. Consequently, Equation (2) $\Psi \equiv \Theta$ becomes

$$\Theta_{\mathbf{i}}^{n+1} = LE_{\mathbf{i}}(\Theta). \tag{3}$$

Given (3) is evaluated prior to momenta, the buoyancy term in the vertical momentum equation $\frac{1}{g}\frac{\Theta'}{\overline{\Theta}}$ is calculated explicitly at t^{n+1}, in the spirit of Runge–Kutta schemes (cf. Smolarkiewicz and Margolin, 1993). Here, Θ' is the difference between Θ and the ambient profile Θ_e, and $\overline{\Theta}$ denotes the hydrostatic reference potential temperature (cf. Section 2b in Clark and Farley, 1984, for a discussion of the reference state).

In the implicit option of the model algorithm, $\Psi \equiv \Theta'$ and $R^{\Theta'} \equiv \mathbf{v}\cdot\nabla\Theta_e$, thereby replacing (3) with

$$\Theta'|_{\mathbf{i}}^{n+1} = LE_{\mathbf{i}}(\widetilde{\Theta'}) - 0.5\Delta t(\mathbf{v}^{n+1}\cdot\nabla\Theta_e)_{\mathbf{i}}. \tag{4}$$

The entropy Equation (4) is solved simultaneously with the momentum equations — via formulating and solving an elaborate elliptic problem for pressure, cf. Smolarkiewicz *et al.* (2004) for discussion — whereupon the buoyancy term is integrated implicitly over $t \in [t^n, t^{n+1}]$ using the trapezoidal rule.

3. Experimental setup

The ambient-state potential temperature is specified as $\Theta_e = \Theta_0 \exp(N^2/g)z$ with $N = 0.01\ \mathrm{s}^{-1}$. The ambient (and initial) profiles u_e and v_e are prescribed as

$$(u_e, v_e) = \begin{cases} (u_0, 0) & \text{if } h \le z < z_1 \\ u_0(\sin\alpha, \cos\alpha) & \text{if } z_1 \le z \le z_2 \\ (0, u_0) & \text{if } z_2 < z \le H \end{cases} \tag{5}$$

with $u_0 = 15\ \mathrm{ms}^{-1}$, $\alpha = \pi/4(1 + \cos\pi(z - z_1/z_2 - z_1))$, $z_1 = 4$ km, $z_2 = 6$ km, and $H = 24$ km altitude, respectively. The minimum ambient Richardson number $Ri_e = 0.31$ at $z = 5$ km suggests marginal flow instability within the shear layer.[2]

The model equations were solved on a regular mesh with $\Delta x = \Delta y$, and temporal increment $\Delta t = 30$ s, over the 6 h of the simulated time. The surface orography is a bell-shaped mountain with height $h(x, y) = h_0(1 + (r/a)^2)^{-3/2}$ where $h_0 = 500$ m, $a = 20$ km and r denotes the horizontal radial distance from the centre of the mountain. The model domain $830 \times 830 \times 24\ \mathrm{km}^3$ was resolved with $416 \times 416 \times 161$ grid intervals, to reconcile with the results of COAMPS. At the lateral and vertical boundaries, gravity waves absorbers attenuate the solution towards the environmental background profiles.

4. Results

In the following, we summarize the results obtained with various options of the numerical solver. The two principal variations discussed are the implicit versus explicit treatment of gravity waves in the fully nonlinear model cast in terrain-following coordinates. These were supplemented with a series of sensitivity studies of the solution on grid staggering, accuracy of the advection scheme, convergence threshold of the elliptic solver, linearizations of various terms in the governing equations, subgrid-scale closures,[3] and the dependence on the temporal and reduced spatial resolution[4].

[2] For three-dimensional unidirectional shear, $Ri_e = 1$ is the transition value, see, e.g. Miles (1986).

[3] As a default, all simulations are performed with the implicit large-eddy-simulation (ILES) approach, where the required subgrid-scale dissipation is provided by the truncation terms of the NFT schemes; cf. Domaradzki *et al.*, 2003, and the references therein.

[4] The experiments with $\delta t \in [1, 40]$ s were considered, while the spatial resolution has been only halved in the horizontal.

Figure 1 juxtaposes the vertical velocity field at $z = 6.0$ km, i.e. right at the top of the shear layer, for the implicit and explicit solver options.[5] The explicit simulations evince small-scale up and downdrafts downstream of the mountain. These structures appear both above and below the shear layer throughout the model depth, Figure 2. In the implicit run, such structures are sporadic above the shear layer and are weaker below. Our sensitivity studies reveal that qualitative aspects of both solutions are robust, although the amplitude of the structures may depend on numerical details. The results in Figures 1 and 2 are shown after 6 h of integration time. For longer times, the discrepancy of the two solutions amplifies, as the small-scale features spread over the model domain in the explicit runs. The corresponding results generated with three different explicit models (COAMPS™, Hodur, 1997, the Clark model, Clark *et al.*, 2000, and the model described in Sharman and Wurtele, 1983, respectively) are consistent with our explicit solution.

5. Discussion

Comparing the implicit and explicit numerical results, it is clear that the two schemes generate solutions that contain qualitatively different features. In the vicinity of the mountain, where the solution is dominated by the vertically propagating hydrostatic gravity wave, the two results agree closely (panels a and b in Figure 2). This illustrates that the overall accuracy of different numerical approximations is about the same. However, in the lee, the explicit solution evinces wave packets with shorter horizontal wavelengths. Above the shear layer, the packets propagate energy away in the vertical; and are trapped below. They appear excited in regions characterized by the local Richardson number $Ri \leq 1.0$ within the shear layer (Figure 2). We speculate that these are signatures of poorly resolved Kelvin–Helmholtz waves.

With four consistent predictions, from four independent numerical models, and the physical appearance of the explicit results, one might be tempted to dismiss the implicit solution. However, we contend that this is the trustworthy result. First, the trapezoidal rule is known to be more accurate than predictor-corrector schemes. In particular, our implicit algorithm does reproduce the correct result in the stringent gravity-wave test of Schär *et al.* (2002), cf. Wedi and Smolarkiewicz (2003); whereas the explicit scheme bifurcates into the spurious state (cf. Klemp *et al.*, 2003). Second, the implicit solution is similar to the linearized-model results from the Sharman code. Third, with the inclusion of a subgrid-scale TKE closure of Schumann (1991) (see Margolin *et al.*, 1999), both models smooth out the regions of unstable Richardson number and a solution is produced resembling the implicit result. On the other hand, if we increase the mountain height — viz. amplify the instability within the shear layer — the fine-scale gravity-wave structures become apparent in the implicit algorithm as well. And fourth, the explicit code produces results similar to the implicit code if the depth of the shear layer is increased and so that $Ri_e > 1.0$ everywhere.

With relentless advances in computer technology, numerical models are more and more often employed to capture fine scales in broad spectra of atmospheric motions. In particular, much effort has been devoted

[5] To not confuse the resolved features with contingent grid-scale noise, the w field has been filtered for display.

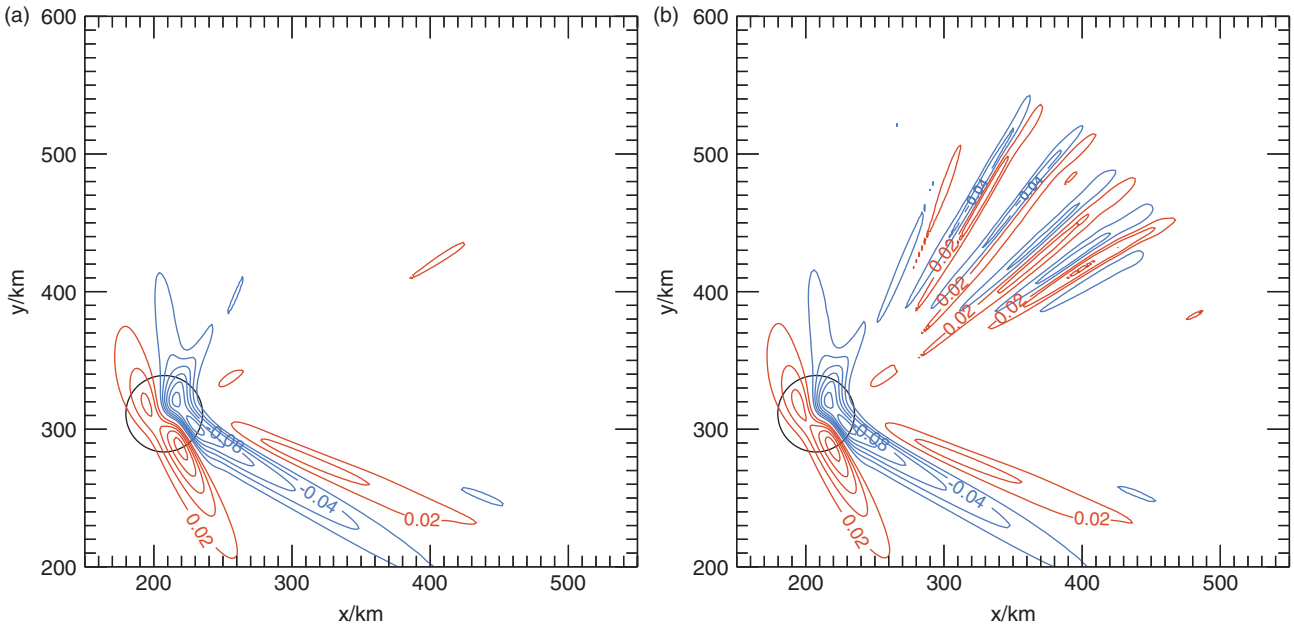

Figure 1. Vertical velocity with contour interval $\Delta w = 0.02$ m/s (red positive, blue negative) at $z = 6$ km altitude, after 6-h integration time for the implicit (a) and explicit simulation (b). The black line marks the 100-m elevation contour line

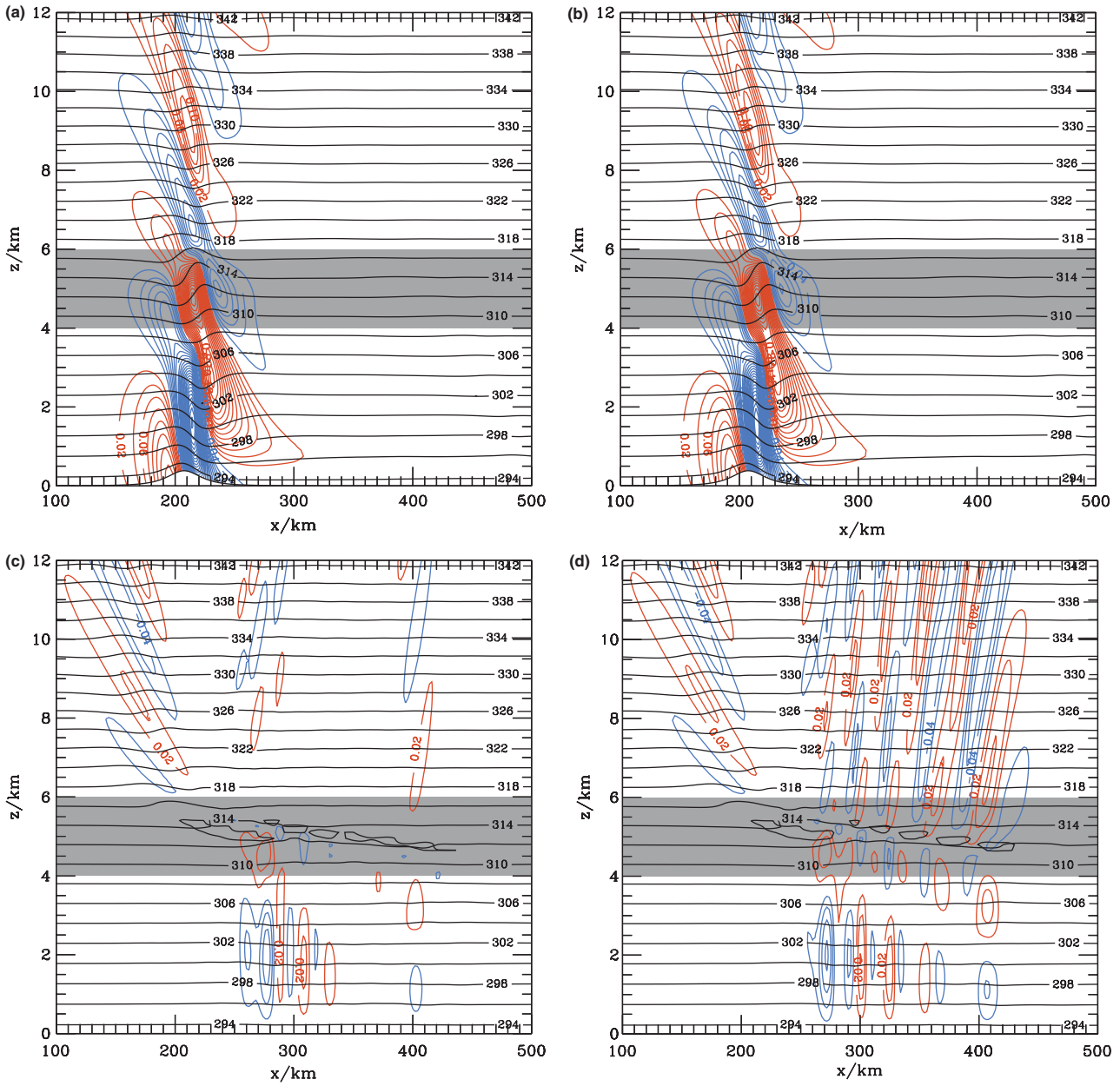

Figure 2. Superposition of vertical velocity (contouring convention as in Figure 1), potential temperature (thin black lines, with contour interval $\Delta\Theta = 2$K), and Richardson number $Ri = 0.25$ (thick black lines), at $y = 320$ km (a, b) and $y = 420$ km (c, d), after 6 h integration time. The implicit and explicit results are shown respectively in plates (a, c) and (b, d). The gray shaded area marks the vertical extent of the shear layer

to simulating clear-air turbulence events (e.g. Clark *et al.*, 2000, and Lane *et al.*, 2004). Clear-air turbulence contains a richness of complex dynamic structures resulting from breaking gravity waves and tangled vortex tubes — local instabilities due to deformation of the ambient flow. Assessing the physical realizability of such structures in numerical model results is difficult, especially since relevant observations are rarely available. This elevates the role of numerical experimentation, supplementing the meteorological case studies. Fluid solvers allowing discriminating numerical options are indispensable tools for estimating the eventual spread of the solutions, thereby promoting advances in computational science and the development of numerical methods.

Acknowledgements

This work was supported in part by the USA Department of Energy 'Climate Change Prediction Program' (CCPP) research initiative. J.D. Doyle was supported by the Office of Naval Research's Program Element 0601153N. COAMPS™ is a trademark of the Naval Research Laboratory. The numerical computations were performed as part of the special project 'Effect of non-hydrostatic gravity waves on the stratosphere above Scandinavia' at the European Centre for Medium Range Weather prediction (ECMWF).

References

Bell JB, Coella P, Glaz HM. 1989. A second-order projection method for the incompressible Navier-Stokes equations. *Journal of Computational Physics* **85**: 257–283.

Clark TL, Farley RD. 1984. Severe downslope windstorm calculations in two and three spatial dimensions using anelastic interactive grid nesting: a possible mechanism for gustiness. *Journal of Atmospheric Sciences* **41**: 329–350.

Clark TL, Hall WD, Kerr RM, Middleton D, Radke L, Ralph M, Neiman PJ, Levinson D. 2000. Origins of aircraft-damaging clear-air turbulence during the 9 December 1992 Colorado downslope windstorm: numerical simulations and comparison with observations. *Journal of Atmospheric Sciences* **57**: 1105–1131.

Domaradzki JA, Xiao Z, Smolarkiewicz PK. 2003. Effective eddy viscosities in implicit large eddy simulations of turbulent flows. *Physics of Fluids* **15**: 3890–3893.

Drikakis D, Smolarkiewicz PK. 2001. On spurious vortical structures. *Journal of Computational Physics* **172**: 309–325.

Drikakis D, Margolin L, Smolarkiewicz PK. 2002. Spurious eddies. *International Journal For Numerical Methods in Fluids* **40**: 313–322.

Grabowski WW, Smolarkiewicz PK. 2002. A multiscale anelastic model for meteorological research. *Monthly Weather Review* **130**: 939–956.

Héreil P, Laprise R. 1996. Sensitivity of internal gravity waves solutions to the time step of a semi-implicit semi-Lagrangian nonhydrostatic model. *Monthly Weather Review* **124**: 972–999.

Hodur RM. 1997. The naval research laboratory's coupled ocean/atmosphere mesoscale prediction system (COAMPS). *Monthly Weather Review* **125**: 1414–1430.

Klemp JB, Skamarock WC, Fuhrer O. 2003. Numerical consistency of metric terms in terrain-following coordinates. *Monthly Weather Review* **131**: 1229–1239.

Lane TP, Doyle JD, Plougonven R, Shapiro MA, Sharman RD. 2004. Observations and numerical simulations of inertia-gravity waves and shearing instabilities in the vicinity of a jet stream. *Journal of Atmospheric Sciences* **61**: 2692–2706.

Margolin LG, Smolarkiewicz PK, Sorbjan Z. 1999. Large-eddy simulations of convective boundary layers using nonoscillatory differencing. *Physica D* **133**: 390–397.

Miles J. 1986. Richardson's criterion for the stability of stratified shear flow. *Physics of Fluids* **29**: 3470–3471.

Prusa JM, Smolarkiewicz PK. 2003. An all-scale anelastic model for geophysical flows: dynamic grid deformation. *Journal of Computational Physics* **190**: 601–622.

Schär C, Leuenberger D, Fuhrer O, Lüthi C, Girard A. 2002. New terrain-following vertical coordinate formulation for atmospheric prediction models. *Monthly Weather Review* **130**: 2459–2480.

Schumann U. 1991. Subgrid length-scales for large-Eddy simulation of stratified turbulence. *Theoretical and Computational Fluid Dynamics* **2**: 279–290.

Sharman RD, Wurtele MG. 1983. Ship waves and lee waves. *Journal of Atmospheric Sciences* **40**: 396–427.

Shutts GJ, Gadian A. 1999. Numerical simulations of orographic gravity waves in flows which back with height. *Quarterly Journal of the Royal Meteorological Society* **125**: 2743–2765.

Smolarkiewicz PK, Clark TL. 1986. The multidimensional positive definite advection transport algorithm: further development and applications. *Journal of Computational Physics* **67**: 396–438.

Smolarkiewicz PK, Margolin LG. 1993. On forward-in-time differencing for fluids: extension to a curvilinear framework. *Monthly Weather Review* **121**: 1847–1859.

Smolarkiewicz PK, Margolin LG. 1997. On forward-in-time differencing for fluids: an Eulerian/semi-Lagrangian nonhydrostatic model for stratified flows. *Atmospheric Ocean Special* **35**: 127–152.

Smolarkiewicz PK, Margolin LG. 1998. MPDATA: a finite-difference solver for geophysical flows. *Journal of Computational Physics* **140**: 459–480.

Smolarkiewicz PK, Prusa JM. 2005. Towards mesh adaptivity for geophysical turbulence: continuous mapping approach. *International Journal for Numerical Methods in Fluids* **47**: 789–801.

Smolarkiewicz PK, Temperton C, Thomas SJ, Wyszogrodzki AA. 2004. Spectral preconditioners for nonhydrostatic atmospheric models: extreme applications. In ECMWF Seminar Series on Recent Developments in Numerical Methods for Atmospheric and Ocean Modelling, 6–10 September 2004, Reading, UK (online: http://www.ecmwf.int/publications/library).

Wedi NP, Smolarkiewicz PK. 2003. Extending Gal-Chen and Somerville terrain-following coordinate transformation on time-dependent curvilinear boundaries. *Journal of Computational Physics* **193**: 1–20.

